Effect of HSP90AB1 on the local immune response of hepatocellular carcinoma and it relationship to prognosis

Keywords

HCC, HSP90AB1, immunotherapy, PD-1, CD8, prognosis

Abstract

Background: HSP90AB1 (heat shock protein 90 kDa alpha, class B, member 1) assists folding proteins and the inhibition of HSP90AB1 is expected to effectively solve the problem of heat shock response of the inhibition of HSP90. The underlying mechanism of the effect of HSP90AB1 on the local immune response against tumors is still unclear. Materials and methods: In this study, we analyzed the effect of HSP90AB1 on immune cell infiltration in HCC tissues. Then, we analyzed the immunoregulatory genes associated with HSP90AB1 and selected KDR\MICB\TNFRSF4 genes to establish a prognostic model. And the prognostic model was verified in the ICGC database and TCGA database. Results: We found that the inhibition of HSP90AB1 could increase the infiltration of CD8 T cells and other immune cells in the HCC tissues. We also found that the inhibition of HSP90AB1 could improve the prognosis of patients with HCC. Conclusion: The inhibition of HSP90AB1 is expected to improve the prognosis of patients with HCC and increase local immune cell infiltration.

Introduction

Hepatocellular carcinoma (HCC) is the seventh most frequently occurring cancer globally and the second most common cause of cancer-related mortality(Bray et al. 2018; Rheinbay et al. 2020). The prognosis for HCC is poor worldwide, and the morbidity and mortality are approximately equal. In 2018, the global morbidity of liver cancer was estimated at 9.3 per thousand and the mortality was 8.5 per thousand(Bray et al. 2018). The prevalence of nonalcoholic fatty liver disease (NAFLD)/nonalcoholic steatohepatitis (NASH) is increasing and may soon surpass viral factors as the leading cause of HCC worldwide(McGlynn et al. 2021). With the emergence of immunotherapy for treating HCC, there has been increasing interest in determining the best way to combine immunotherapy with local therapy(Greten et al. 2019). However, the effect of immunotherapy in some patients is poor, and recent studies on enhancing the effect of immunotherapy by other therapeutic means have become a hotspot(Llovet et al. 2018). Among them, the ability of HSP90 inhibitors to improve immunotherapy outcomes has received considerable attention(Proia & Kaufmann 2015).

HSP90AB1 (heat shock protein 90 kDa alpha, class B, member 1), also known as HSP90Beta, is a member of the large HSP family and acts as a molecular chaperone by binding to receptor proteins. It also supports proper protein folding and maintains protein stability. Because receptor proteins can be mutated proteins that degrade without the help of chaperones, heat shock proteins can

also promote tumor formation and cancer cell proliferation(Miyata et al. 2013). Inhibition of the HSP90AB1 function is a promising approach for the treatment of a wide range of diseases(Haase & Fitze 2016), including cancer, and inflammatory and genetic diseases. Inhibition of the Hsp90 protein folding mechanism leads to a combinatorial attack on multiple carcinogenic pathways(Trepel et al. 2010). Seventeen small molecule inhibitors of Hsp90 have entered clinical trials, all of which bind to the N terminus of Hsp90 and exhibit pan-inhibitory activity against all the four Hsp90 subtypes(Khandelwal et al. 2018). Further, Hsp90 C-terminal domain (CTD) inhibitors are promising new agents for cancer treatment because they do not induce the heat shock response associated with Hsp90 N-terminal inhibitors(Tomašič et al. 2020). In the MC-38 syngeneic mouse tumor model, Hsp90 inhibition was found to significantly reduce PD-L1 surface expression on isolated living tumor cells and, in line with recent findings, was found to increase the number of activated CD8+ T cells in the tumor environment(Bae et al. 2013; Zavareh et al. 2021). Previous studies have shown that the inhibition of Hsp90 by ganetespib enhances autologous T-cell killing of patient-derived human melanoma cells in vitro and enhances in vivo responses to both CTLA4 and anti-PD1 therapies(Mbofung et al. 2017). A mechanistic study has shown that the inhibition of Hsp90 leads to the upregulation of the interferon response gene IFIT1, IFIT2, and IFIT3, which is critical for T cells to enhance the killing effect of ganetespib treated melanoma cells(Mbofung et al. 2017). In vivo injection of the

HSP90 inhibitor 17-dimethylaminoethylamino-17-normethoxyglamycin (17-DMAG) in MCA205 tumor-bearing mice slowed tumor growth, enhanced/prolonged tumor cell recognition by anti-EphA2 CD8+ T cells, and reduced the levels of myeloid suppressor cells and regulatory T cells in the tumor microenvironment. In the current study, treatment of EphA2+ tumor cells with the irreversible HSP90 inhibitor 17-DMAG enhances their recognition by EphA2specific CD8+ T cell lines and clones *in vitro*(Kawabe et al. 2009; Rao et al. 2012). 17-DMAG increased CD8+ T cells, decreased double-negative T cells, decreased the CD4/CD8 ratio, and decreased follicular B cells(Shimp et al. 2012). Inhibition of HSP90 leads to greater proteasomal degradation of HER2(erb-b2 receptor tyrosine kinase 2), leading to the display of MHC-enhanced antigenic peptides that are subsequently targeted by CD8+ T cells. The infiltration of T and NK lymphocytes was enhanced in the tumor environment of syngeneic C3H mice. In the absence of immunotherapy, a “high” dose (10 μg) of geldanamycin (GA) reduced tumor growth, whereas a “low” dose (2.5 μg) of GA reduced tumor growth and HER2 expression without reducing the tumor size of syngeneic C3H mice. The DNA vaccine targeting $p185^{neu}$ combined with low GA dose significantly improved the overall survival of syngeneic C3H mice, which was dependent on increasing CD8+ T-lytic cells and reducing CD4+ T cells (possibly reducing Treg cell numbers and allowing more CD8+ killing activity)(Lin et al. 2007). Half of the pleiotropic effect inhibition may allow its use at low levels to enhance the immune

response of tumors via mechanisms including enhanced tumor antigen target decomposition, increased MHC display density, and increased levels of nuclear factor kappa light chain enhancer of activated B cells (NFκB)(Lin et al. 2007) and downstream effects to inhibit tumor microenvironment, and increased expression of natural killer (NK) cells to target. All the previous studies(Graner 2016) that have reported improved immune responses in tumor models after treatment with HSP90 inhibitors used low inhibitor doses, suggesting that low doses of the drug—possibly in combination with the accumulation of preferred drugs in the tumor—may be sufficient to drive molecular changes in the tumor (enhancing immunity) without compromising systemic immunity(Graner 2016). Inhibition of Hsp90 also blocks the proliferation of CD4+ T cells in mouse and human MLRs in vitro(Yun et al. 2011). MHC class I antigen presentation is mediated by the ubiquitin-proteasome degradation pathway and can be enhanced by GA. The infiltration of CD8+ T cells and NK cells was significantly increased in tumor sites. GA sensitizes tumor cells to the cytotoxic effects of lymphocytes. However, GA also has a toxic effect on cultured T cells by downregulating the activity of protein tyrosine kinases in T cells(Lin et al. 2007). Inhibition of Hsp90 can make immunorefractory tumors more sensitive to the T-cell killing but it can block PD-1 expression and reactivate the immune cycle of tumor-responsive T cells(Song et al. 2020). In the oncology setting, the tumor-selective/retention properties of Hsp90 inhibitors allow the use of an intermittent administration regimen, resulting

in effective and sustained chaperone inhibitory activity in the lumen of the tumor, and more limiting systemic immune system drug exposure(Proia & Kaufmann 2015). The HSP90 inhibitor 17-allylamino-17-methoxyglenamycin (17-AAG) has been identified as an effective stimulator of melanoma antigen expression that enhances T-cell tumor recognition in melanoma(Haggerty et al. 2012). Notably, treatment with 17-DMAG and agonistic EphA2 antibodies further enhanced tumor cell recognition by CD8+ T cells(Kawabe et al. 2009). However, the effect of HSP90 inhibitors on the local immune response of liver cancer has not been systematically studied. Therefore, we comprehensively analyzed the effect of HSP90AB1 on the local immune response of liver cancer based on the clinical data obtained from the TCGA database. We specifically identified the local immune cells related to HSP90AB1, screened the immune regulatory genes related to HSP90AB1, and constructed a prognosis model. We verified this prognosis model by using the data obtained from the ICGC database to accurately determine the effect of HSP90AB1 on the local immune response in liver cancer.

Materials and methods

The hepatocellular carcinoma (HCC) transcriptome data were downloaded from the TCGA database(Hutter & Zenklusen 2018), and the data were divided into HCC and normal groups, and the gene ID was converted into gene name. Clinical

data were downloaded and extracted from the TCGA database. The differences in the HSP90AB1 gene expression between the normal and HCC groups were observed (Figure 1). Immune cell infiltration analysis was performed to obtain the number of immune cells from the data of TCGA database, and a bar chart was prepared(Figure 2). Moreover, different immune cells are shown in different colors. To analyze the correlation among the immune cells, we drew the correlation graph to observe the correlation between different immune cells (Figure 3), and further patients can be divided into the normal and HCC groups (Figure 4) to observe the immune cells in the normal and HCC groups. Figure 5 shows the difference between violin maps as well as the contrast difference in immune cells between the normal and HCC groups. TIMER(Li et al. 2017) was used to study the relationship between different copy numbers of the HSP90AB1 gene and immune cells. GSEA(Subramanian et al. 2005) enrichment analysis was performed using the GSEA software to determine the activity of different pathways considering the up-and downregulated expression of the HSP90AB1 gene. Correlation analysis of HSP90AB1 gene expression and lymphocyte count in TISIDB was performed to obtain a correlation heat map of HSP90AB1 gene expression and different lymphocytes in different tumors. Thereafter, a correlation scatter map of HSP90AB1 gene expression and different types of lymphocytes in HCC tissue was obtained. The correlation coefficient between HSP90AB1 gene expression and different lymphocytes was determined. A correlation heat map of

HSP90AB1 gene expression and immunoregulatory genes in different tumors was obtained using TISIDB(Ru et al. 2019). A scatter map of the correlation between different immunoregulatory genes and HSP90AB1 gene expression in HCC tissues was also obtained. The immunoregulatory genes co-expressed with the HSP90AB1 gene were identified. STRING(von Mering et al. 2003) was used to construct a protein interaction network of immunoregulatory genes co-expressed with the HSP90AB1 gene to determine the protein interaction relationships of these genes. Then, the GO function statistics and pathway enrichment analysis of these genes was performed using the Web-based Gene Set Analysis Toolkit(Wang et al. 2013) to identify the functions and significant enrichment pathways in which these genes were involved. The expression data of these immunoregulatory genes were combined with the survival data of clinical patients, and a prognostic analysis was performed to identify the immunoregulatory genes related to the prognosis of patients, based on which a forest map was prepared. These genes were used to construct a prognostic model. According to the expression of prognostic model genes in each patient, the risk score of each patient was calculated. The patients in TCGA database were been divided to 2 groups on an average. Those higher than the median risk score were classified as the high-risk group, while those lower than the median risk score were classified as the low-risk group. Then, a risk curve was drawn, patient groups were prepared, survival status was determined, and high and low risk genes were

identified to determine the relationship between gene expression and patient risk. Univariate and multivariate independent prognostic analysis was performed to determine the factors that could be independently analyzed for prognosis. An ROC curve was plotted to observe the accuracy of different factors in predicting patient survival. A graph was prepared accordingly, and the score of each trait of each patient was obtained according to the scoring scale. The survival rate of patients at different time nodes could be predicted according to the total score. By preparing a calibration curve and observing the proximity of the two curves, we could approximately determine the accuracy of the constructed model for predicting the prognosis of patients. Thereafter, the LIRI-JP file from NOV 27 and 2019 data was downloaded from the ICGC database(Rheinbay et al. 2020) for verification, and the survival difference between the groups with up- and downregulated HSP90AB1 gene expression and the constructed prognosis model were verified.

Results

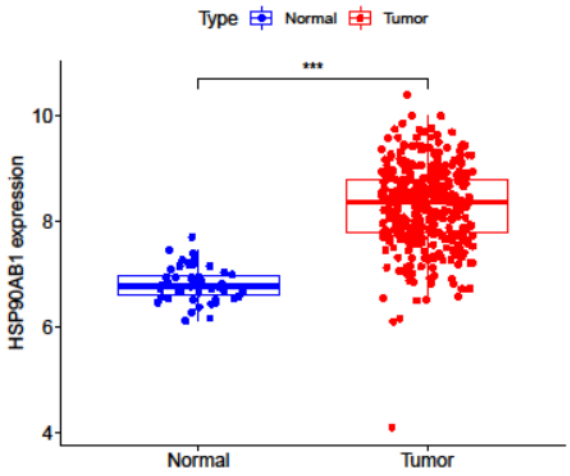

Figure 1. HSP90AB1 gene expression in the HCC group and the normal group.

According to the clinical data of HCC in the TCGA database, HSP90AB1 gene expression in the HCC group was significantly higher than that in the normal group (P <0.001).

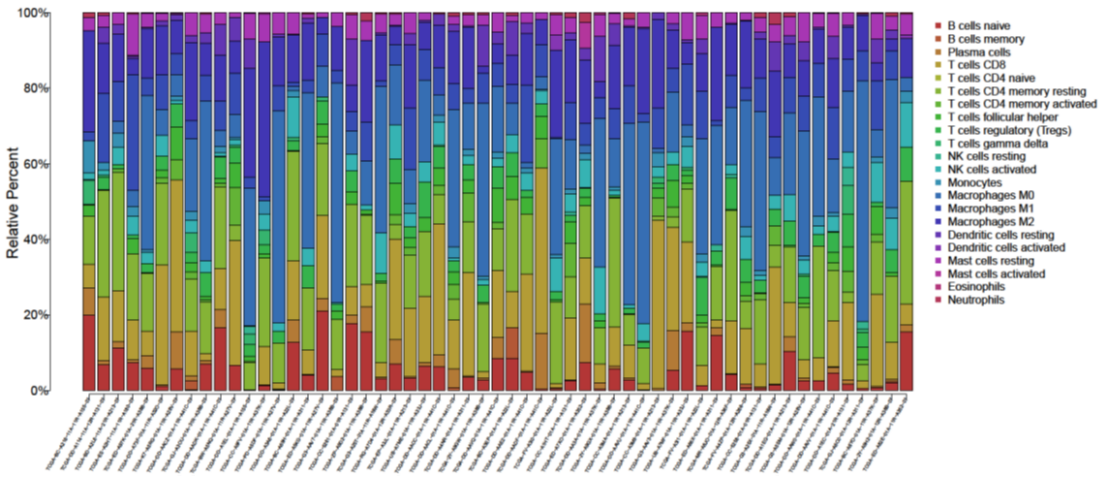

Figure 2. Different immune cell types in each HCC patient.

Figure 2 shows the different immune cell types in each HCC patient in the TCGA database. Different immune cells are represented in different colors, and the number of each immune cell type can also be seen.

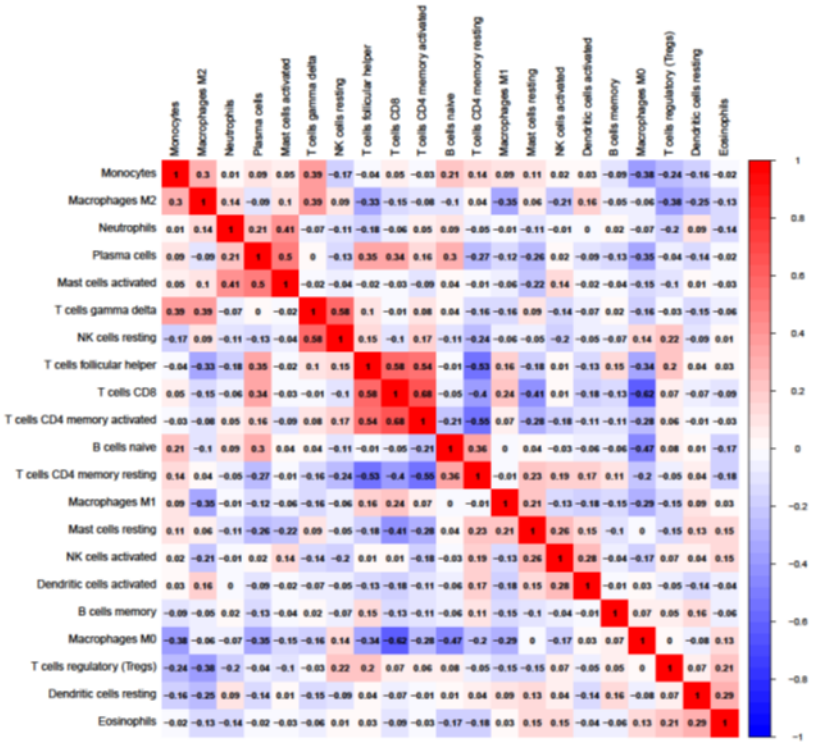

195

196 Figure 3. Heatmap of correlation among different immune cells in the HCC

197 patients.

198 This figure shows the correlation among different immune cells in the HCC

199 patients obtained from the TCGA database. Macrophage M0 cells had the most

200 significant negative correlation with CD8+ T cells, whereas CD4 memory

201 activated T cells had the most significant positive correlation with CD8+ T cells.

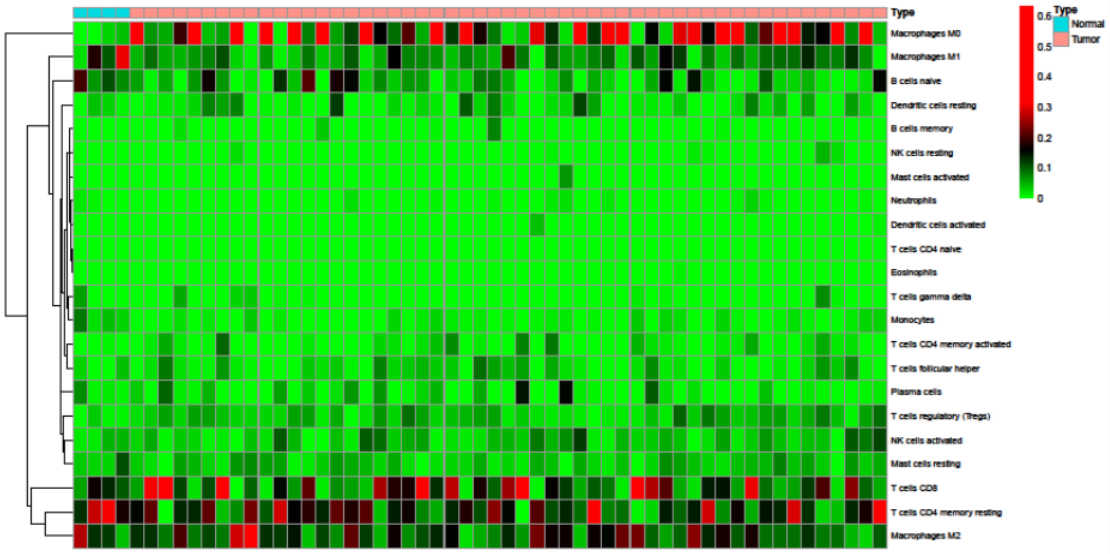

Figure 4. Different immune cells between normal and HCC patients.

The patients were divided into normal and HCC groups in the heat map(Figure 4). The differences in immune cells in both groups are obvious. The Macrophage M0 content in the normal group was significantly lower than that in the HCC group.

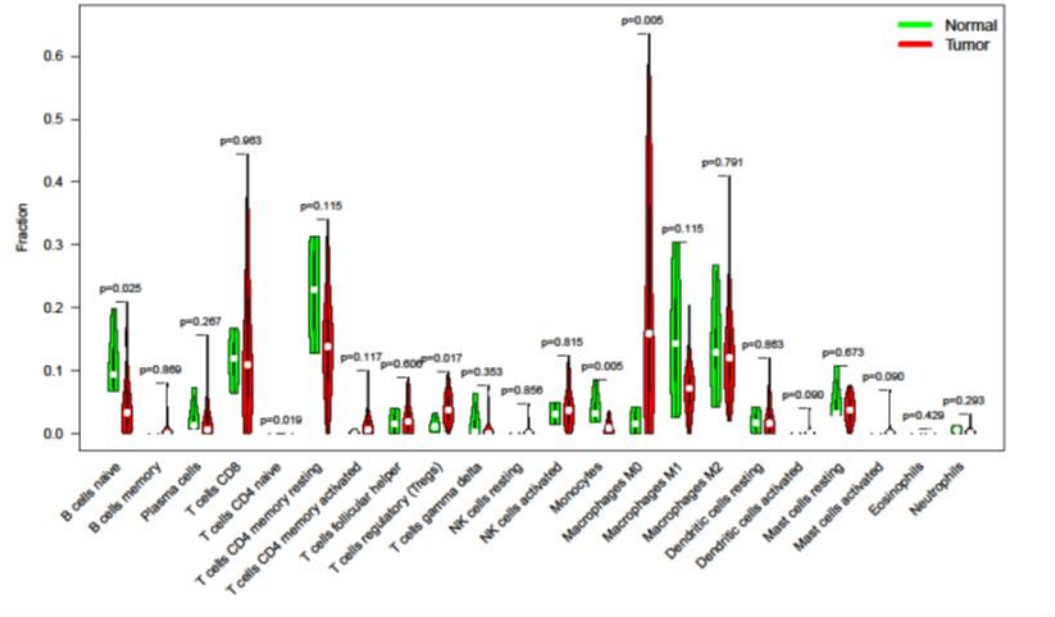

Figure 5. Differences in the infiltration of the immune cells between the normal

and tumor groups.

The numbers of each immune cell type in both the groups were compared to obtain the violin chart of immune cell infiltration, with P values added above each group. The screening of significantly different immune cells was performed according to P values <0.05. The number of Naïve B cells, naïve CD4 T cells, regulatory T cells (Tregs), monocytes, and macrophages M0 were different in both the groups. The numbers of Tregs and macrophages M0 in the HCC group were higher than those in the normal group.

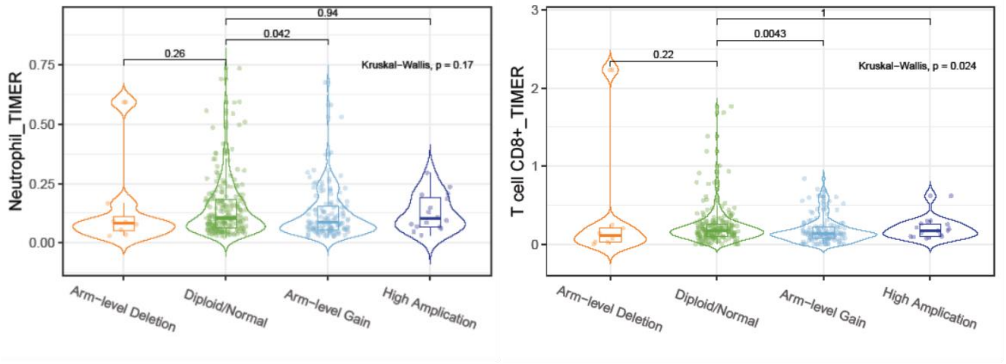

Figure 6. Influence of different copy numbers of HSP90AB1 for neutrophil and CD8+ T cell infiltration in HCC.

The infiltration of neutrophils and CD8+ T cells was decreased when HSP90AB1 was at the Arm-level Gain($P < 0.05$) in Figure 6.

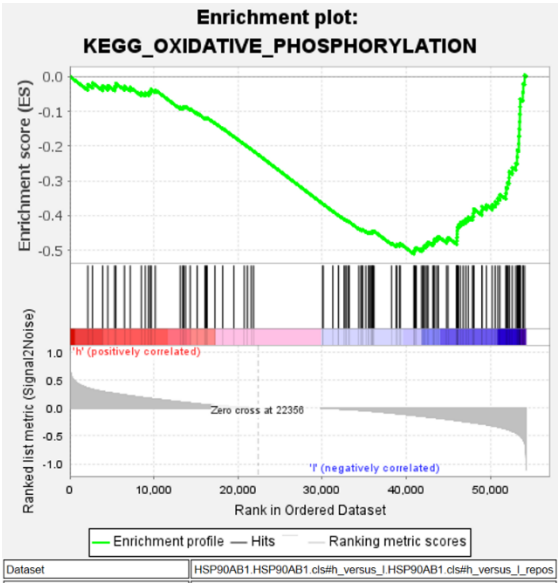

Dataset	HSP90AB1.HSP90AB1.cls#h_versus_l.HSP90AB1.cls#h_versus_l_repos
Phenotype	HSP90AB1.cls#h_versus_l_repos
Upregulated in class	l
GeneSet	KEGG_OXIDATIVE_PHOSPHORYLATION
Enrichment Score (ES)	-0.5101812
Normalized Enrichment Score (NES)	-1.4851172
Nominal p-value	0.037623763

Figure 7. GSEA enrichment analysis of HSP90AB1.

The oxidative-phosphorylation pathway was active when HSP90AB1 gene expression was downregulated ($p < 0.05$) according to the GSEA enrichment analysis(Figure 7).

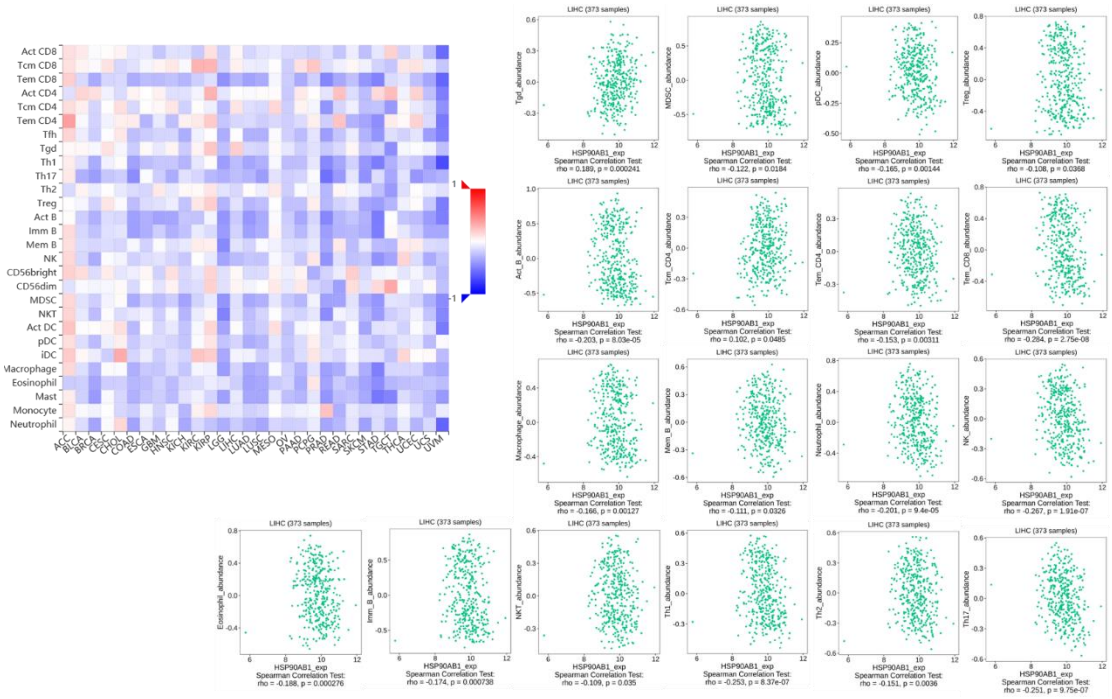

228

229 Figure 8. Correlation between HSP90AB1 gene expression and lymphocyte

230 count.

231 The correlation between HSP90AB1 gene expression and lymphocyte count

232 was analyzed, and screening of significantly related lymphocyte count with the

233 HSP90AB1 gene expression was conducted according to P values <0.05 in

234 Figure 8. In HCC, TGD cells and TCM_CD4 cells were positively correlated with

235 HSP90AB1 gene expression. The numbers of NK cells, Tem_CD8 cells, Th1 cells,

236 Th17 cells, MDSC cells, pDC cells, Treg cells, Act_B cells, Tem_CD4 cells,

237 macrophages, Mem_B cells, Neutrophils, Eosinophils, Imm_B cells, NKT cells,

238 and Th2 cells were negatively correlated with HSP90AB1 gene expression.

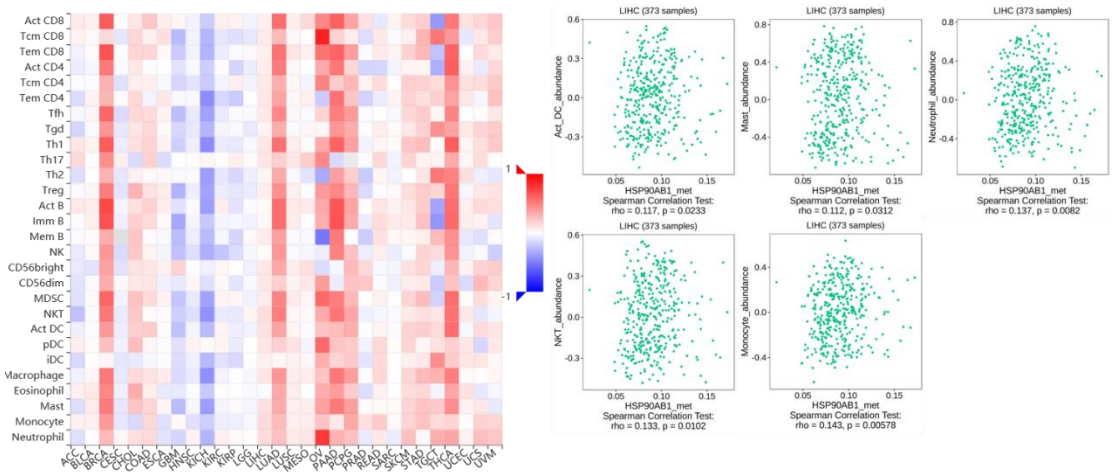

Figure 9. Correlation between the methylation of the HSP90AB1 gene and lymphocyte count.

The correlation between the methylation of the HSP90AB1 gene and lymphocyte count was analyzed. The screening was performed according to P values <0.05. In HCC, the numbers of ACT_DC cells, mast cells, neutrophils, NKT cells, and monocytes were positively correlated with HSP90AB1 gene methylation.

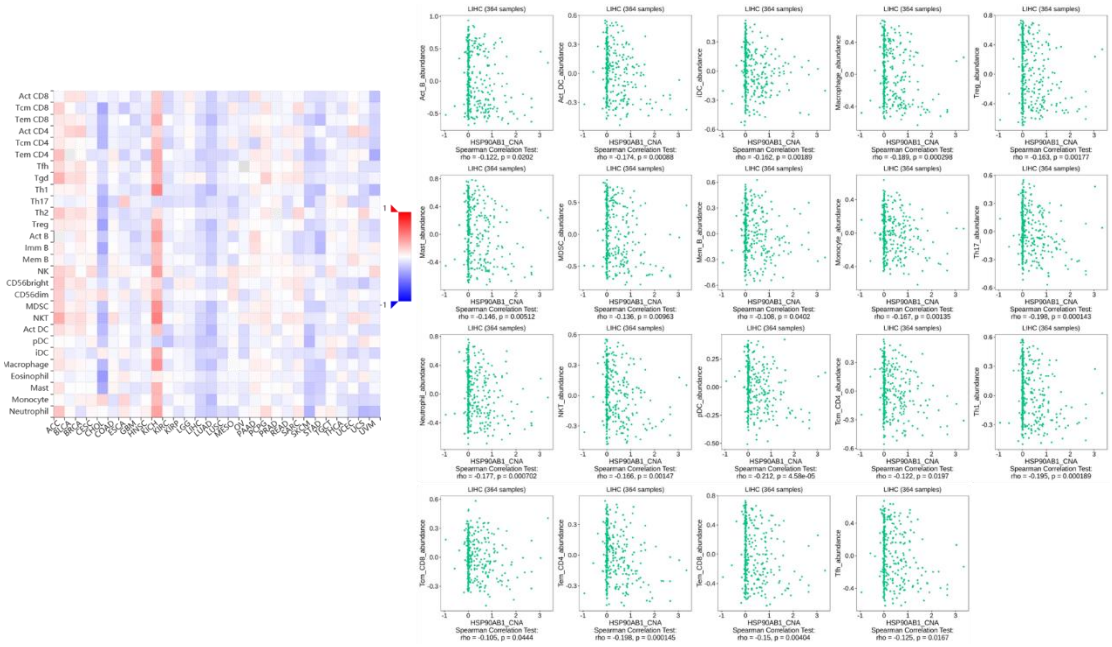

247

248 Figure 10. Correlation between the copy number of the HSP90AB1 gene and

249 lymphocyte count.

250 The correlation between the copy number of the HSP90AB1 gene and

251 lymphocyte count was analyzed in Figure 10. The screening was performed

252 according to P values <0.05. The numbers of ACT_B cells, ACT_DC cells, IDC

253 cells, macrophages, Tregs, mast cells, MDSC cells, MEM_B cells, monocytes,

254 Th17 cells, neutrophils, NKT cells, PDC cells, TCM_CD4 cells, Th cells 1,

255 TCM_CD8 cells, TEM_CD4 cells, TEM_CD8 cells, and TFH cells were negatively

256 correlated with the copy number of the HSP90AB1 gene.

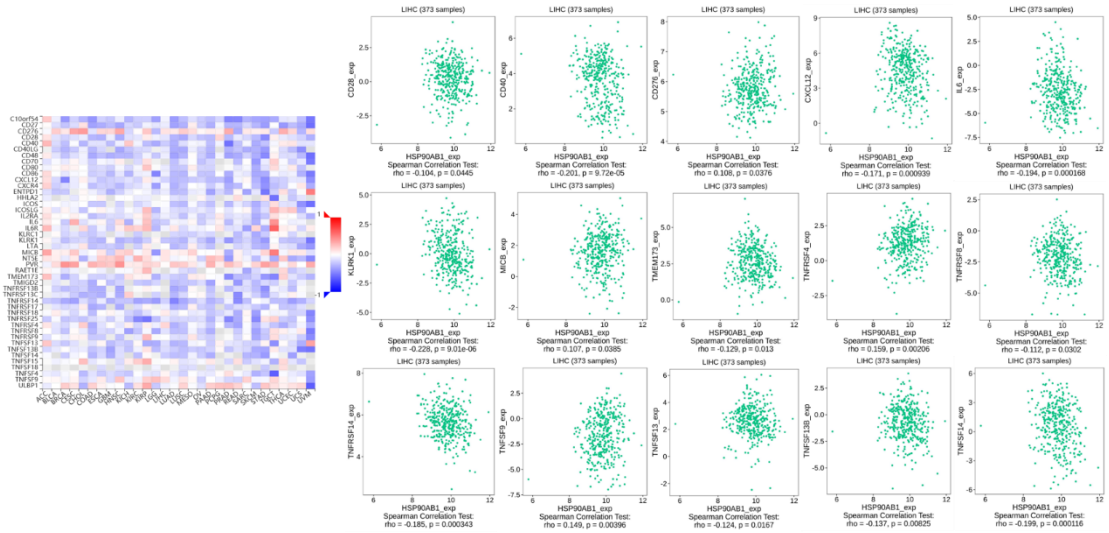

Figure 11. Correlational analysis between the HSP90AB1 gene and immune-stimulating genes.

Correlation analysis was performed between the HSP90AB1 gene and immune-stimulating genes, and screening was conducted according to P values <0.05. The following genes were negatively correlated with the HSP90AB1 gene: CD28, CD40, CXCL12, IL6, KLRK1, TMEM173, TNFRSF8, TNFRSF14, TNFSF13, TNFSF13B, TNFSF14, and HSP90AB1. The CD276, MICB, TNFRSF4, and TNFSF9 genes were positively correlated with the HSP90AB1 gene.

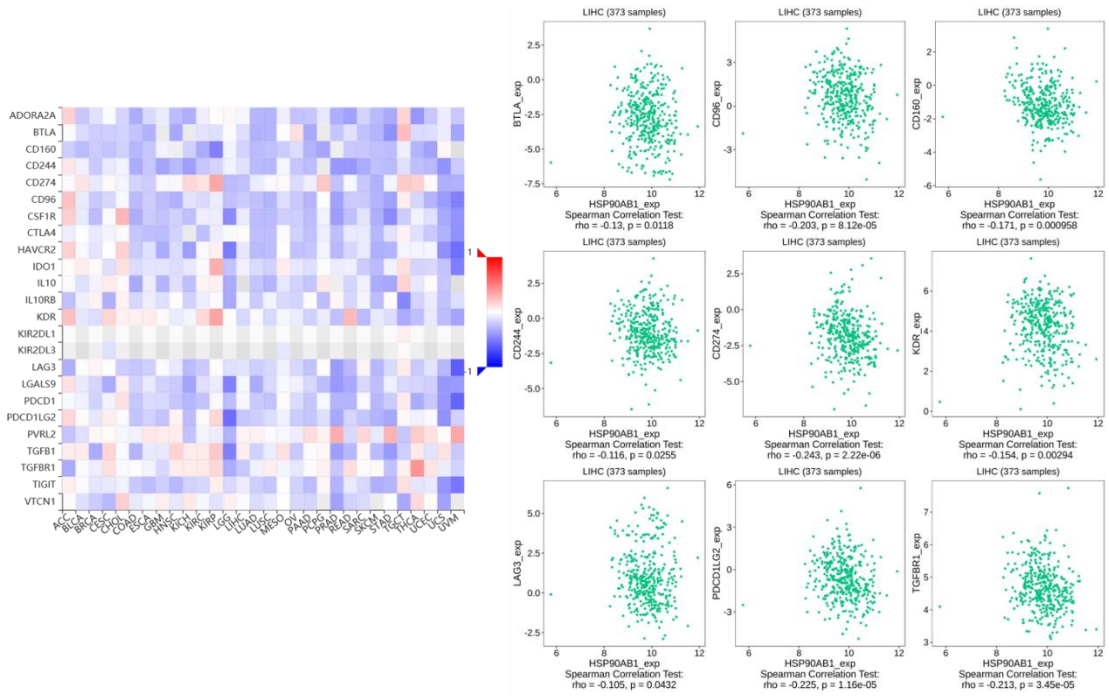

Figure 12. Correlational analysis between the HSP90AB1 gene and immunosuppressive genes.

The correlation between the HSP90AB1 gene and immunosuppressive genes was analyzed. The screening was performed according to P values <0.05. The following genes were negatively correlated with the HSP90AB1 gene: BTLA, CD96, CD160, CD244, CD274, KDR, LAG3, PDCD1LG2, and TGFbr1.

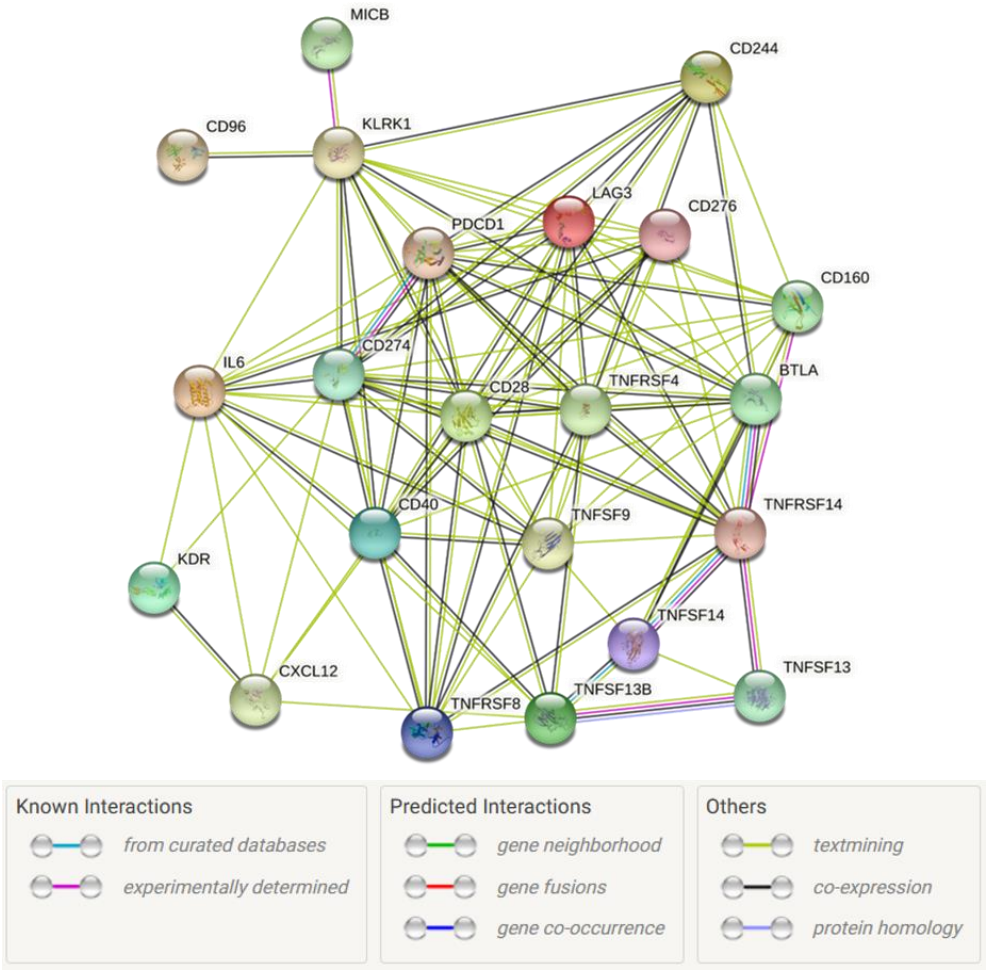

Figure 13. Protein-interaction network of immune-stimulating genes and immunosuppressive genes related to the HSP90AB1 gene.

The immune-stimulating genes related to the HSP90AB1 gene and immunosuppressive genes were used to construct a protein interaction network, and the different interaction relationships among the genes were connected with colorful lines.

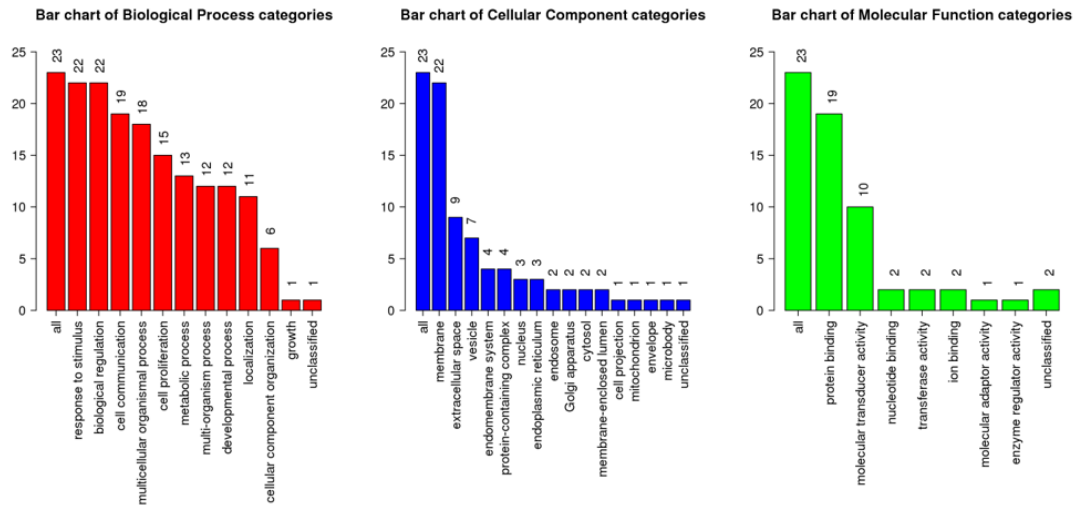

Figure 14. GO function statistical analysis on genes in the protein-interaction network.

Using the Web-based Gene Set Analysis Toolkit, GO function statistical analysis was performed on genes in the protein interaction network. Functional genes were filtered according to FDR values of <0.05, and the number of genes involved in each function is represented at the top.

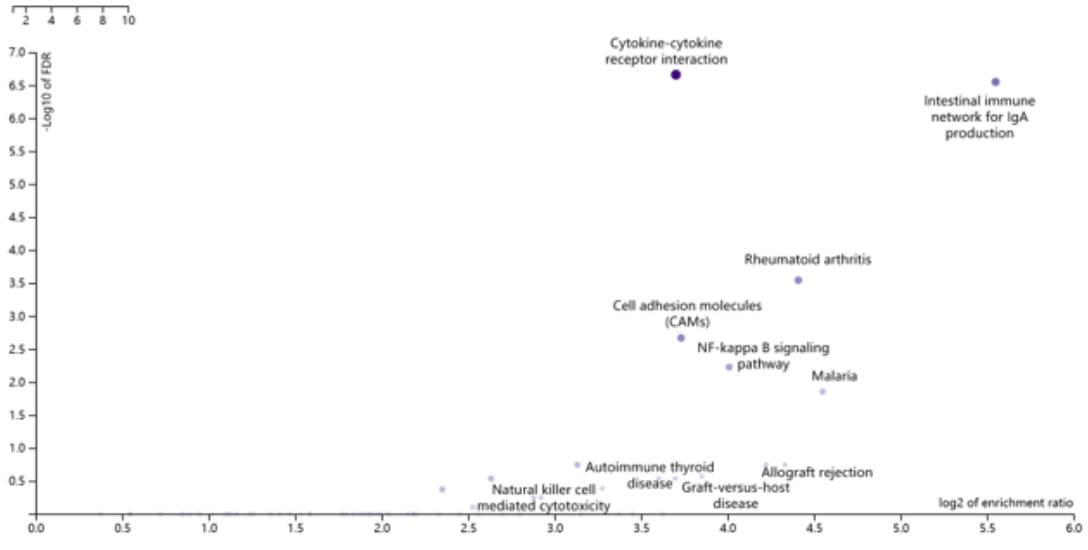

Figure 15. Pathways of significantly enriched genes identified based on the GO

function statistical analyses.

The names of the pathways of significantly enriched genes identified based on GO function statistical analysis of the protein interaction network using the Web-based Gene Set Analysis Toolkit are labeled in the volcano map. The significant enrichment pathways included cytokine-cytokine receptor interaction, intestinal immune network for IgA production, rheumatoid arthritis, and cell plasma molecules (CAMS), NF-kappa B signaling pathway, malaria, etc.

Table 1. The genes related to the prognosis of HCC patients in the protein-interaction network.

id	HR	HR.95L	HR.95H	p value
KDR	0.773	0.635	0.941	0.010
CD276	1.284	1.019	1.619	0.034
MICB	1.292	1.019	1.638	0.035
TNFRSF4	1.321	1.053	1.656	0.016

The genes related to the prognosis of patients with HCC were screened in **Table 1** from the protein interaction network(Figure 13) ($P < 0.05$). As shown in the table, the KDR gene was a prognostically low-risk gene, whereas CD276, MICB, and TNFRSF4 genes were prognostically high-risk genes.

Table 2. The prognostic model of selected prognosis-related genes.

id	coef	HR	HR.95L	HR.95H	p value
KDR	-0.226	0.798	0.655	0.972	0.025
MICB	0.217	1.243	0.981	1.575	0.072
TNFRSF4	0.223	1.249	0.993	1.572	0.057

The prognostic model was constructed by further screening the selected prognosis-related genes. The coefficient of each gene is given in the **Table 2**. The risk score of each patient was obtained according to the model formula.

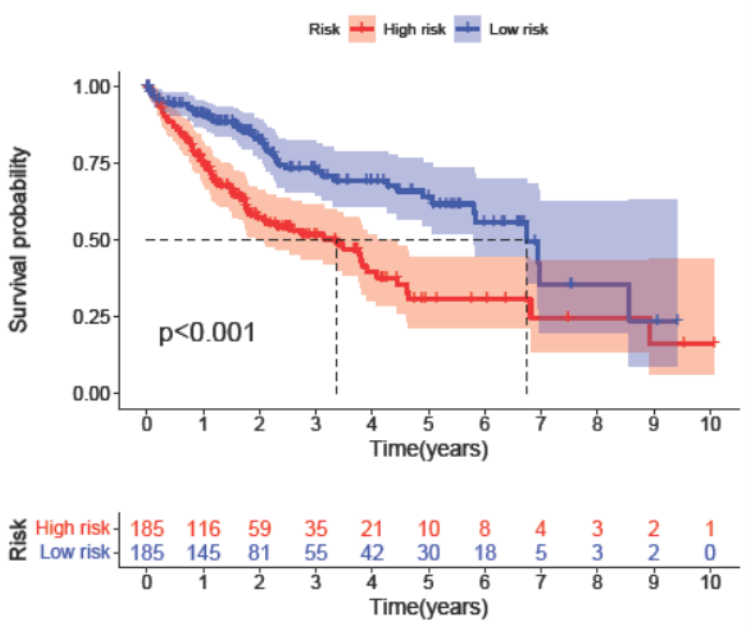

Figure 16. The survival curve of high- and low-risk groups classified according to the prognostic model of HCC patients in the TCGA database.

The survival curves of patients were plotted according to the high- and low-risk groups classified according to the prognostic model in Figure 16. The prognosis of patients in the low-risk group was significantly better than that in the high-risk

group (P < 0.001).

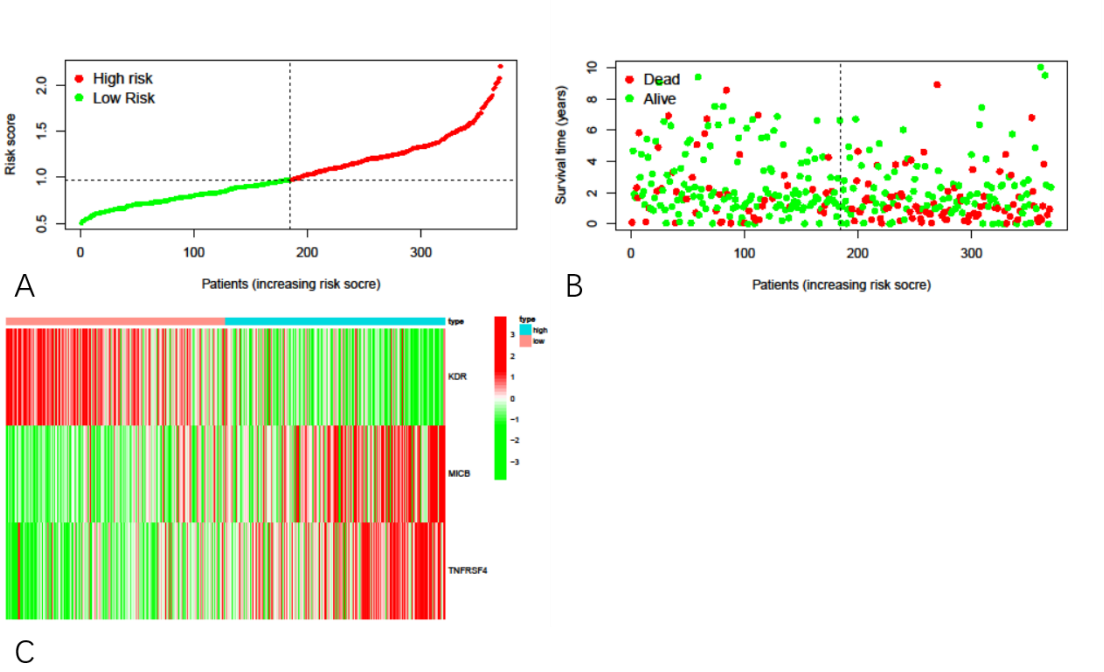

Figure 17. The risk curve of high- and low-risk groups classified according to the prognostic model of HCC patients in the TCGA database.

The risk curve of patients was drawn. As shown in Figure 17A, the risk scores of patients gradually increased from left to right, and the patients were divided into the high- and low-risk groups based on the median risk scores. Figure 17B shows that from left to right, patients' risk scores showed an increasing trend. The higher the risk score, the greater the mortality. Figure 17C shows that, in the high-risk group, the *KDR* gene expression was low, whereas the expression of *MICB* and *TNFRSF4* genes were high, indicating that *KDR* is a low-risk gene, while *MICB* and *TNFRSF4* are high-risk genes for HCC development in the TCGA database.

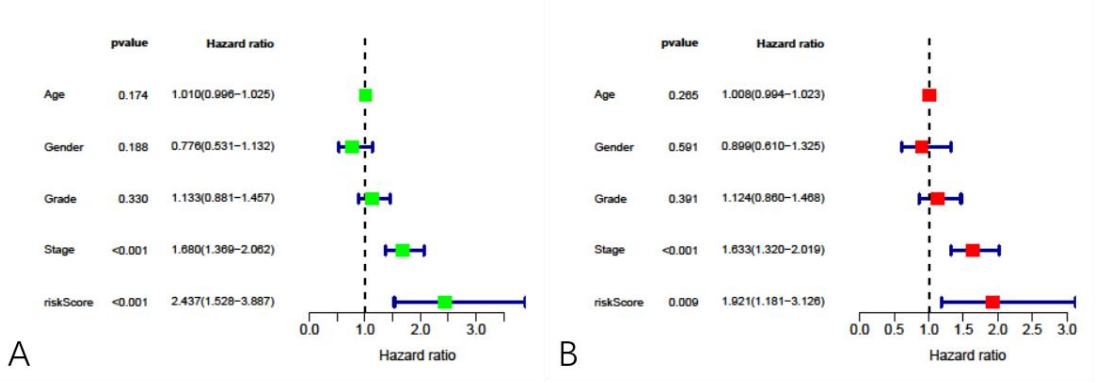

Figure 18. Single-factor and multi-factor independent prognostic analyses of the established prognostic model in the TCGA database.

An independent prognostic analysis of the established prognostic model was performed. Figure 18A showed the forest plot of single-factor independent prognostic analysis, and Figure 18B shows the forest plot of multi-factor independent prognostic analysis. Both the P values in the prognostic model were less than 0.01, indicating that the prognostic model could be used for prognostic analysis independently of other traits.

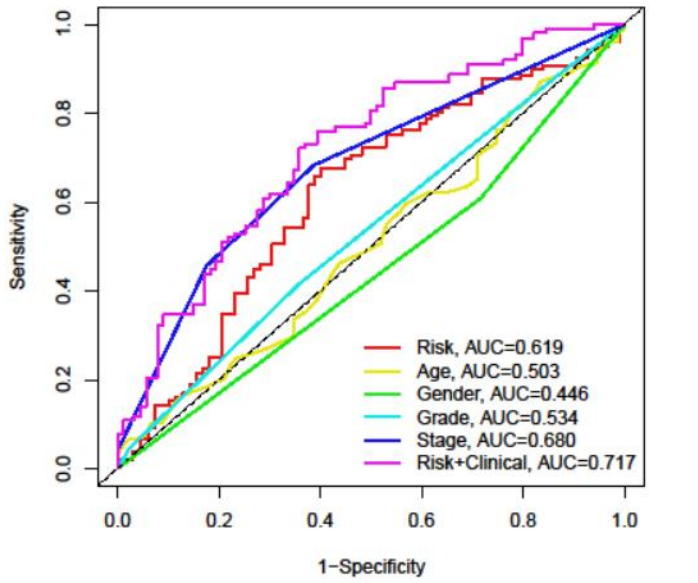

335

336 Figure 19. The ROC curve of the prognostic model and other clinical traits in the

337 TCGA database.

338 The ROC curve(Figure 19) showed that the area under the Risk+Clinical curve

339 was the largest, and the area under the Risk curve was slightly smaller than the

340 area under the Stage curve, indicating that the prognosis model could predict the

341 survival of patients accurately when combined with other clinical traits.

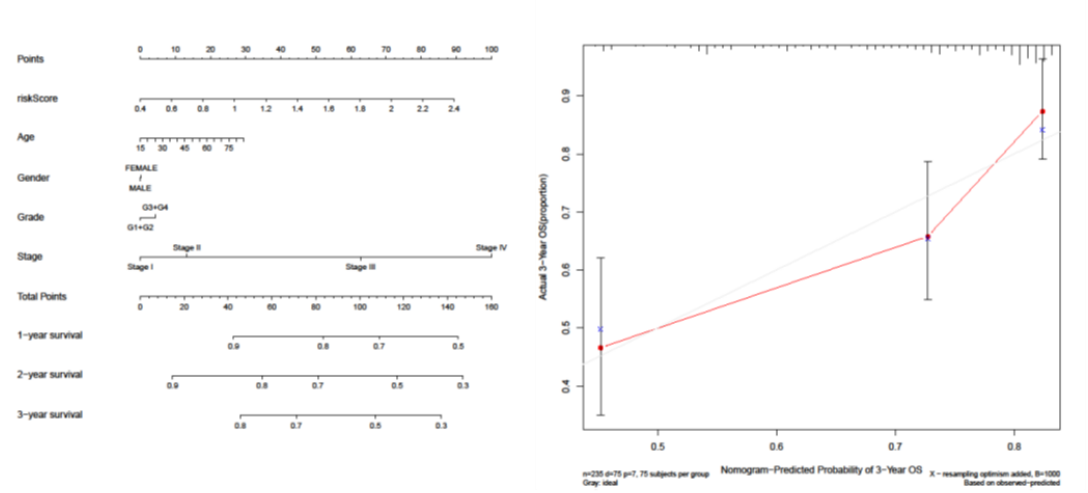

A B

Figure 20. The nomogram and calibration curves of the prognostic model in the TCGA database.

Figure 20A depicts a nomogram used to predict HCC patient survival analysis. Each clinical trait score of the patients can be obtained using the single-factor scoring scale, and the scores can be added to obtain the comprehensive score of the patients, according to which the comprehensive score can be used to predict one-year, two-year, and three-year survival rates of patients. The calibration curve is shown in Figure 20B. The two curves are close to each other, indicating that the prediction of the constructed prognosis model is accurate.

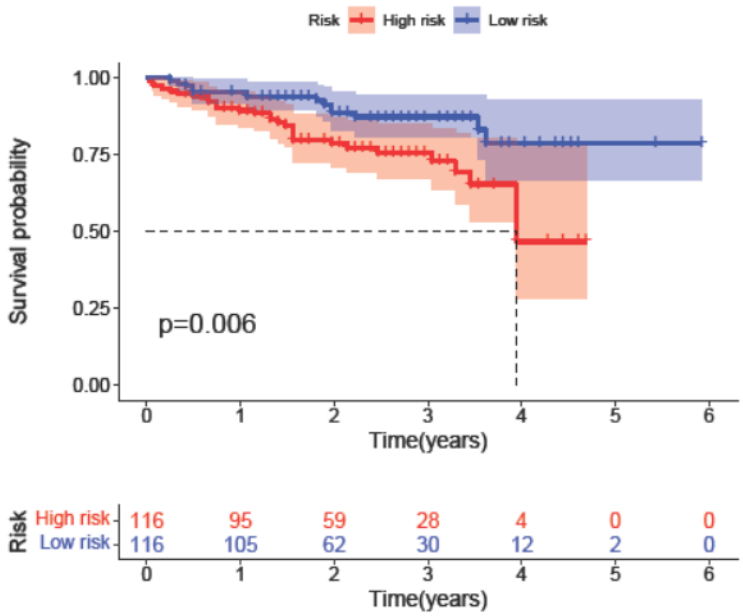

Figure 21. The survival curve of high- and low-risk groups classified according to the prognostic model of HCC patients in the ICGC database.

According to the established prognosis model, patients identified according to the ICGC database were divided into low- and high-risk groups, and survival curves were obtained(Figure 21). A P value <0.05 indicated that the prognosis in the low-risk group was significantly better than that in the high-risk group.

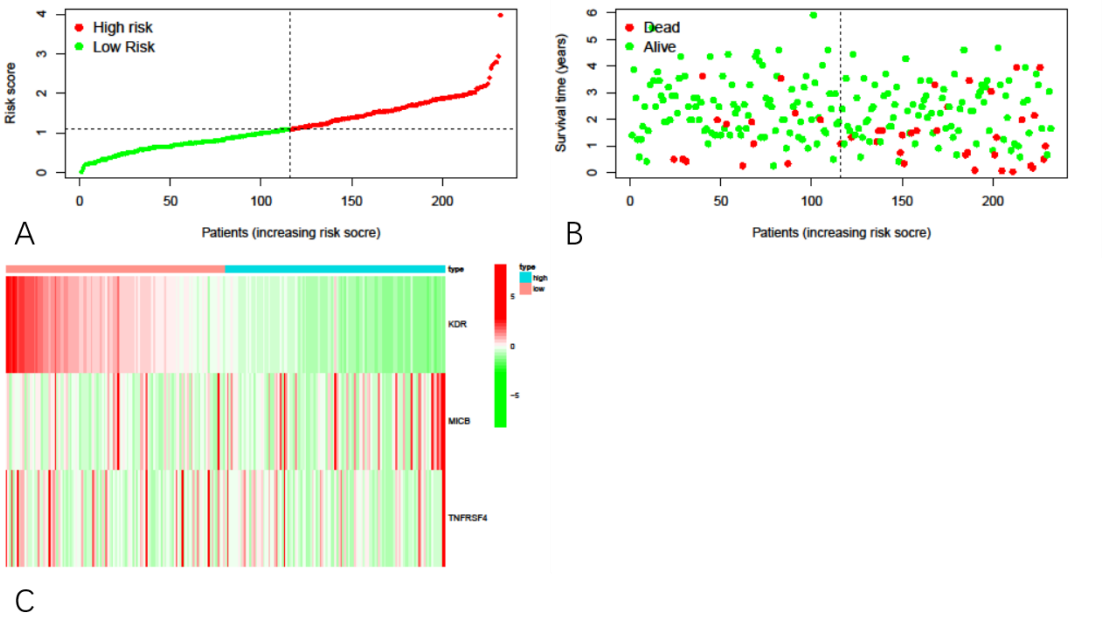

Figure 22. The risk curve of high- and low-risk groups classified according to the prognostic model of HCC patients in the ICGC database.

In the ICGC database, the risk curve, the abscissa of which is the patients in order, gradually increases from left to right. The ordinate in Figure 22A is the risk score. In Figure 22B, the vertical axis is the patient survival time. From left to right, the number of patients dying increased. Figure 22C is a risk heat map showing the expression of KDR, MICB, and TNFRSF4 genes in the high- and low-risk groups, whereas KDR gene expression was found to be low in the high-risk group.

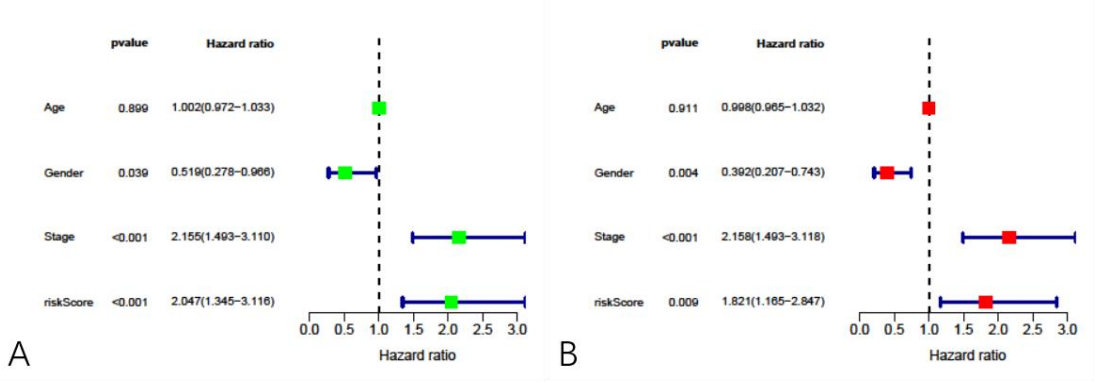

Figure 23. Single-factor and multi-factor independent prognostic analyses of the established prognostic model in the ICGC database.

An independent prognostic analysis of the data obtained from the ICGC database was performed to determine whether the constructed model could be used as an independent prognostic factor independent of other clinical traits. Figure 23A shows the forest plot of univariate independent prognostic analysis. The Stage and riskScore with P values <0.001 indicate that the prognostic analysis can be performed independently of other traits. Figure 23B shows the forest plot of multi-factor independent prognostic analysis. The Stage and riskScore with P values <0.01 indicate that the prognostic analysis can be performed independently of other traits. In conclusion, Stage and riskScore can be used for prognostic analysis independently of other traits.

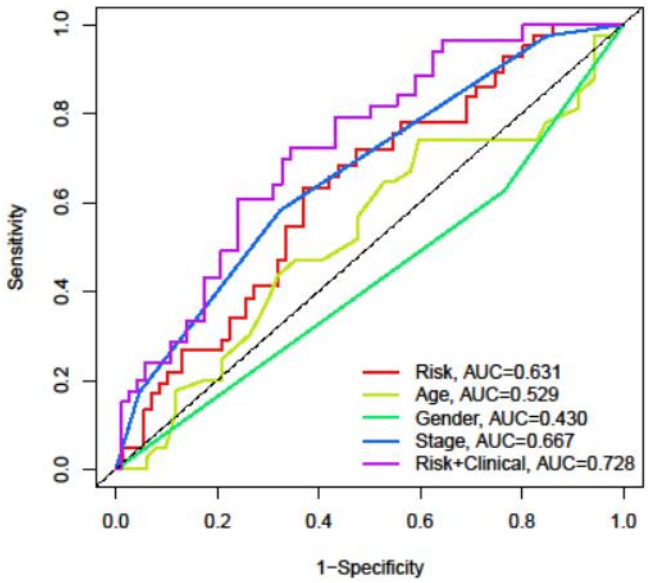

Figure 24. The ROC curve of the prognostic model and other clinical traits in the ICGC database.

In the ROC curve(Figure 24) of the ICGC database, the larger the area under the curve, the higher the accuracy of predicting the survival of patients using this model. The abscissa represents the false positive rate (1-specificity) and the ordinate represents the true positive rate (sensitivity). The area under the model was smaller than the area under staging but larger than the area under other traits. The area was the largest when the model was combined with other clinical traits, indicating that the model combined with other clinical traits could predict the survival of patients accurately.

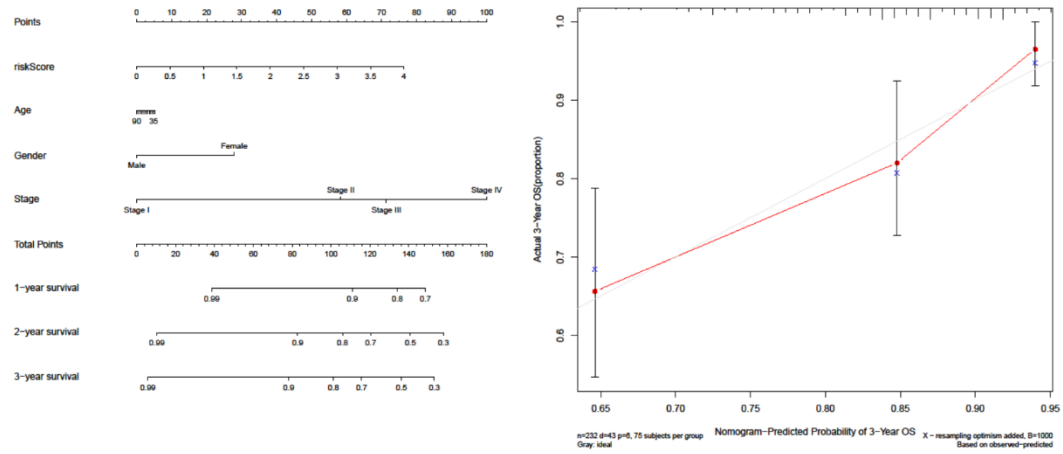

A B

Figure 25. The nomogram and calibration curves of the prognostic model in the ICGC database.

In the ICGC database, a single factor-scoring scale was used to obtain the scores of each clinical trait of the patients, and the scores were added to obtain comprehensive scores for predicting the survival rate of the patients(Figure 25). The abscissa of the calibration curve is the mortality predicted by the model and the ordinate is the actual mortality rate. The two curves are very close to each other, indicating that the model's prediction is accurate.

Discussion

Recently, some studies have reported the enhanced effect of HSP90 inhibitors on tumor immunotherapy(Kawabe et al. 2009; Rao et al. 2012; Zhang et al. 2021). However, the pan-inhibition of HSP90 inhibitors has limited their widespread use. Some studies have been exploring the possibility of reducing the side effects of

Hsp90 inhibitors, one of which is targeting the HSP90AB1 subtype(Khandelwal et al. 2018). Therefore, we comprehensively analyzed the effect of HSP90AB1 on the local immune response against HCC by using data obtained from the TCGA database. Many immune cells infiltrated in HCC were found to be negatively correlated with Hsp90β. The most prominent of these cells were several CD8+ T cells, which was similar to the results of previous studies on Hsp90 inhibitors(Bae et al. 2013; Zavareh et al. 2021). Inhibition of Hsp90β is expected to considerably increase the infiltration of local killer immune cells in HCC and enhance the therapeutic effect of immune checkpoint inhibitors. Further studies are needed to explore the relevant effects. We also identified the immunomodulatory genes related to Hsp90β and screened several immunostimulating genes and immunosuppressive genes to construct a prognosis model. The prognosis of patients whose data was available in the TCGA database was analyzed, and we found that the inhibition of Hsp90β could significantly improve the prognosis of patients. NK cells, Tem_CD8 cells, Th1 cells, Th17 cells, MDSC cells, pDC cells, Treg cells, Act_B cells, Tem_CD4 cells, macrophages, Mem_B cells, neutrophils, eosinophils, Imm_B cells, NKT cells, and Th2 cells were negatively correlated with HSP90AB1 gene expression in the local microenvironment of HCC. In addition, the infiltration of neutrophils and CD8+ T cells decreased when HSP90AB1 gained an additional copy ($P < 0.05$), which was consistent with the results of previous studies on HSP90(Kawabe et al. 2009; Rao et al. 2012; Zhang

et al. 2021). HSP90AB1 inhibition can increase the infiltration of CD8+ T cells in the local microenvironment of HCC. GSEA enrichment analysis showed that the oxidative phosphorylation pathway was active when HSP90AB1 expression was low, whereas M2 macrophages mainly relied on oxidative phosphorylation to obtain energy(Griffiths et al. 2017). Moreover, our current understanding showed that aerobic glycolysis is a marker of CD8+ T cell activation, and immature and memory (TMEM) cells tend to rely on oxidative phosphorylation; so, mitochondrial metabolism is a key determinant of CD8+ TMEM cell development(Raud et al. 2018). Most tumor-infiltrating T cells exhibit an eventual depletion phenotype marked by loss of self-renewal. In the activated T cells, the inhibition of mitochondrial oxidative phosphorylation was sufficient to inhibit the proliferation and upregulation of genes associated with T cell failure. On the other hand, the prevention of mitochondrial oxidative stress during chronic T cell stimulation leads to sustained T cell proliferation and induction of genes associated with stem-like T progenitor cells. In addition, a treatment that maintains the REDOX balance can promote T cell self-renewal and enhance anti-tumor immunity(Vardhana et al. 2020). We used the screened MICB(Ferrari de Andrade et al. 2018), KDR(Llovet et al. 2018), and TNFRSF4(Buchan et al. 2018) genes to construct the prognostic model, in which KDR was a low-risk gene and MICB, TNFRSF4 genes are high-risk genes for HCC development according to the TCGA database, but the degree of genetic risk is not clear in the ICGC database. KDR is a low-risk

prognostic gene in clinical data, and the results are highly consistent in the clinical data obtained from the two databases. However, previous studies have reported that the KDR gene can promote the angiogenesis of mouse liver cell cancer cells and is correlated with tumor progression, which is contrary to the results obtained from the analysis of clinical data in the present study. This discrepancy may be caused by the limitations of the current experimental model, and hence, further studies are needed. The prognosis model constructed according to the immunoregulatory genes related to HSP90AB1 can better predict the survival of patients when it is taken into consideration with other clinical traits including age, gender, grade, stage, and the reliability of this model has been verified based on the information given in the ICGC database.

Conclusion

In conclusion, HSP90AB1 inhibition can increase the infiltration of CD8+ T cells in local HCC and reduce the side effects of traditional Hsp90 inhibitors, thus allowing them to be used as potential therapeutic agents to enhance the efficacy of immunotherapy. In summary, the prognosis model constructed based on KDR, MICB, and TNFRSF4 gene expression and other clinical traits can better predict the prognosis of patients with HCC.

Acknowledgemengt

Declarations of interest: there is no conflict of interest.

Reference

Bae J, Munshi A, Li C, Samur M, Prabhala R, Mitsiades C, Anderson KC, and Munshi NC. 2013. Heat shock protein 90 is critical for regulation of phenotype and functional activity of human T lymphocytes and NK cells. *J Immunol* 190:1360-1371. 10.4049/jimmunol.1200593

Bray F, Ferlay J, Soerjomataram I, Siegel RL, Torre LA, and Jemal A. 2018. Global cancer statistics 2018: GLOBOCAN estimates of incidence and mortality worldwide for 36 cancers in 185 countries. *CA Cancer J Clin* 68:394-424. 10.3322/caac.21492

Buchan SL, Rogel A, and Al-Shamkhani A. 2018. The immunobiology of CD27 and OX40 and their potential as targets for cancer immunotherapy. *Blood* 131:39-48. 10.1182/blood-2017-07-741025

Ferrari de Andrade L, Tay RE, Pan D, Luoma AM, Ito Y, Badrinath S, Tsoucas D, Franz B, May KF, Jr., Harvey CJ, Kobold S, Pyrdol JW, Yoon C, Yuan GC, Hodi FS, Dranoff G, and Wucherpfennig KW. 2018. Antibody-mediated inhibition of MICA and MICB shedding promotes NK cell-driven tumor immunity. *Science* 359:1537-1542. 10.1126/science.aao0505

Graner MW. 2016. HSP90 and Immune Modulation in Cancer. *Adv Cancer Res* 129:191-224. 10.1016/bs.acr.2015.10.001

Greten TF, Mauda-Havakuk M, Heinrich B, Korangy F, and Wood BJ. 2019. Combined locoregional-immunotherapy for liver cancer. *J Hepatol* 70:999-1007. 10.1016/j.jhep.2019.01.027

Griffiths HR, Gao D, and Pararasa C. 2017. Redox regulation in metabolic programming and inflammation. *Redox Biol* 12:50-57. 10.1016/j.redox.2017.01.023

Haase M, and Fitze G. 2016. HSP90AB1: Helping the good and the bad. *Gene* 575:171-186. 10.1016/j.gene.2015.08.063

Haggerty TJ, Dunn IS, Rose LB, Newton EE, and Kurnick JT. 2012. A screening assay to identify agents that enhance T-cell recognition of human melanomas. *Assay Drug Dev Technol* 10:187-201. 10.1089/adt.2011.0379

Hutter C, and Zenklusen JC. 2018. The Cancer Genome Atlas: Creating Lasting Value beyond Its Data. *Cell* 173:283-285. 10.1016/j.cell.2018.03.042

Kawabe M, Mandic M, Taylor JL, Vasquez CA, Wesa AK, Neckers LM, and Storkus WJ. 2009. Heat shock protein 90 inhibitor 17-dimethylaminoethylamino-17-demethoxygeldanamycin enhances EphA2+ tumor cell recognition by specific CD8+ T cells. *Cancer Res* 69:6995-7003. 10.1158/0008-5472.CAN-08-4511

Khandelwal A, Kent CN, Balch M, Peng S, Mishra SJ, Deng J, Day VW, Liu W, Subramanian C, Cohen M, Holzbeierlein JM, Matts R, and Blagg BSJ. 2018. Structure-guided design of an Hsp90β N-terminal isoform-selective inhibitor. *Nat Commun* 9:425. 10.1038/s41467-017-02013-1

Li T, Fan J, Wang B, Traugh N, Chen Q, Liu JS, Li B, and Liu XS. 2017. TIMER: A Web Server for

Comprehensive Analysis of Tumor-Infiltrating Immune Cells. *Cancer Res* 77:e108-e110. 10.1158/0008-5472.Can-17-0307

Lin CC, Tu CF, Yen MC, Chen MC, Hsieh WJ, Chang WC, Chang WT, and Lai MD. 2007. Inhibitor of heat-shock protein 90 enhances the antitumor effect of DNA vaccine targeting clients of heat-shock protein. *Mol Ther* 15:404-410. 10.1038/sj.mt.6300014

Llovet JM, Montal R, Sia D, and Finn RS. 2018. Molecular therapies and precision medicine for hepatocellular carcinoma. *Nat Rev Clin Oncol* 15:599-616. 10.1038/s41571-018-0073-4

Mbofung RM, McKenzie JA, Malu S, Zhang M, Peng W, Liu C, Kuiatse I, Tieu T, Williams L, Devi S, Ashkin E, Xu C, Huang L, Zhang M, Talukder AH, Tripathi SC, Khong H, Satani N, Muller FL, Roszik J, Heffernan T, Allison JP, Lizee G, Hanash SM, Proia D, Amaria R, Davis RE, and Hwu P. 2017. HSP90 inhibition enhances cancer immunotherapy by upregulating interferon response genes. *Nat Commun* 8:451. 10.1038/s41467-017-00449-z

McGlynn KA, Petrick JL, and El-Serag HB. 2021. Epidemiology of Hepatocellular Carcinoma. *Hepatology* 73 Suppl 1:4-13. 10.1002/hep.31288

Miyata Y, Nakamoto H, and Neckers L. 2013. The therapeutic target Hsp90 and cancer hallmarks. *Curr Pharm Des* 19:347-365. 10.2174/138161213804143725

Proia DA, and Kaufmann GF. 2015. Targeting Heat-Shock Protein 90 (HSP90) as a Complementary Strategy to Immune Checkpoint Blockade for Cancer Therapy. *Cancer Immunol Res* 3:583-589. 10.1158/2326-6066.Cir-15-0057

Rao A, Taylor JL, Chi-Sabins N, Kawabe M, Gooding WE, and Storkus WJ. 2012. Combination therapy with HSP90 inhibitor 17-DMAG reconditions the tumor microenvironment to improve recruitment of therapeutic T cells. *Cancer Res* 72:3196-3206. 10.1158/0008-5472.CAN-12-0538

Raud B, McGuire PJ, Jones RG, Sparwasser T, and Berod L. 2018. Fatty acid metabolism in CD8(+) T cell memory: Challenging current concepts. *Immunol Rev* 283:213-231. 10.1111/imr.12655

Rheinbay E, Nielsen MM, Abascal F, Wala JA, Shapira O, Tiao G, Hornshøj H, Hess JM, Juul RI, Lin Z, Feuerbach L, Sabarinathan R, Madsen T, Kim J, Mularoni L, Shuai S, Lanzós A, Herrmann C, Maruvka YE, Shen C, Amin SB, Bandopadhayay P, Bertl J, Boroevich KA, Busanovich J, Carlevaro-Fita J, Chakravarty D, Chan CWY, Craft D, Dhingra P, Diamanti K, Fonseca NA, Gonzalez-Perez A, Guo Q, Hamilton MP, Haradhvala NJ, Hong C, Isaev K, Johnson TA, Juul M, Kahles A, Kahraman A, Kim Y, Komorowski J, Kumar K, Kumar S, Lee D, Lehmann KV, Li Y, Liu EM, Lochovsky L, Park K, Pich O, Roberts ND, Saksena G, Schumacher SE, Sidiropoulos N, Sieverling L, Sinnott-Armstrong N, Stewart C, Tamborero D, Tubio JMC, Umer HM, Uusküla-Reimand L, Wadelius C, Wadi L, Yao X, Zhang CZ, Zhang J, Haber JE, Hobolth A, Imielinski M, Kellis M, Lawrence MS, von Mering C, Nakagawa H, Raphael BJ, Rubin MA, Sander C, Stein LD, Stuart JM, Tsunoda T, Wheeler DA, Johnson R, Reimand J, Gerstein M, Khurana E, Campbell PJ, López-Bigas N, Weischenfeldt J, Beroukhim R, Martincorena I, Pedersen JS, and Getz G. 2020. Analyses of non-coding somatic drivers in 2,658 cancer whole genomes. *Nature* 578:102-111. 10.1038/s41586-020-1965-x

Ru B, Wong CN, Tong Y, Zhong JY, Zhong SSW, Wu WC, Chu KC, Wong CY, Lau CY, Chen I, Chan NW, and Zhang J. 2019. TISIDB: an integrated repository portal for tumor-immune system

interactions. *Bioinformatics* 35:4200-4202. 10.1093/bioinformatics/btz210

Shimp SK, 3rd, Chafin CB, Regna NL, Hammond SE, Read MA, Caudell DL, Rylander M, and Reilly CM. 2012. Heat shock protein 90 inhibition by 17-DMAG lessens disease in the MRL/lpr mouse model of systemic lupus erythematosus. *Cell Mol Immunol* 9:255-266. 10.1038/cmi.2012.5

Song KH, Oh SJ, Kim S, Cho H, Lee HJ, Song JS, Chung JY, Cho E, Lee J, Jeon S, Yee C, Lee KM, Hewitt SM, Kim JH, Woo SR, and Kim TW. 2020. HSP90A inhibition promotes anti-tumor immunity by reversing multi-modal resistance and stem-like property of immune-refractory tumors. *Nat Commun* 11:562. 10.1038/s41467-019-14259-y

Subramanian A, Tamayo P, Mootha VK, Mukherjee S, Ebert BL, Gillette MA, Paulovich A, Pomeroy SL, Golub TR, Lander ES, and Mesirov JP. 2005. Gene set enrichment analysis: a knowledge-based approach for interpreting genome-wide expression profiles. *Proc Natl Acad Sci U S A* 102:15545-15550. 10.1073/pnas.0506580102

Tomašič T, Durcik M, Keegan BM, Skledar DG, Zajec Ž, Blagg BSJ, and Bryant SD. 2020. Discovery of Novel Hsp90 C-Terminal Inhibitors Using 3D-Pharmacophores Derived from Molecular Dynamics Simulations. *Int J Mol Sci* 21. 10.3390/ijms21186898

Trepel J, Mollapour M, Giaccone G, and Neckers L. 2010. Targeting the dynamic HSP90 complex in cancer. *Nat Rev Cancer* 10:537-549. 10.1038/nrc2887

Vardhana SA, Hwee MA, Berisa M, Wells DK, Yost KE, King B, Smith M, Herrera PS, Chang HY, Satpathy AT, van den Brink MRM, Cross JR, and Thompson CB. 2020. Impaired mitochondrial oxidative phosphorylation limits the self-renewal of T cells exposed to persistent antigen. *Nat Immunol* 21:1022-1033. 10.1038/s41590-020-0725-2

von Mering C, Huynen M, Jaeggi D, Schmidt S, Bork P, and Snel B. 2003. STRING: a database of predicted functional associations between proteins. *Nucleic Acids Res* 31:258-261. 10.1093/nar/gkg034

Wang J, Duncan D, Shi Z, and Zhang B. 2013. WEB-based GEne SeT AnaLysis Toolkit (WebGestalt): update 2013. *Nucleic Acids Res* 41:W77-83. 10.1093/nar/gkt439

Yun TJ, Harning EK, Giza K, Rabah D, Li P, Arndt JW, Luchetti D, Biamonte MA, Shi J, Lundgren K, Manning A, and Kehry MR. 2011. EC144, a synthetic inhibitor of heat shock protein 90, blocks innate and adaptive immune responses in models of inflammation and autoimmunity. *J Immunol* 186:563-575. 10.4049/jimmunol.1000222

Zavareh RB, Spangenberg SH, Woods A, Martinez-Pena F, and Lairson LL. 2021. HSP90 Inhibition Enhances Cancer Immunotherapy by Modulating the Surface Expression of Multiple Immune Checkpoint Proteins. *Cell Chem Biol* 28:158-168 e155. 10.1016/j.chembiol.2020.10.005

Zhang Y, Ware MB, Zaidi MY, Ruggieri AN, Olson BM, Komar H, Farren MR, Nagaraju GP, Zhang C, Chen Z, Sarmiento JM, Ahmed R, Maithel SK, El-Rayes BF, and Lesinski GB. 2021. Heat Shock Protein-90 Inhibition Alters Activation of Pancreatic Stellate Cells and Enhances the Efficacy of PD-1 Blockade in Pancreatic Cancer. *Mol Cancer Ther* 20:150-160. 10.1158/1535-7163.Mct-19-0911